Optical Engineering 44(3), 036202 (March 2005)

Bidirectional reflectance distribution function and directional-hemispherical reflectance of a martian regolith simulant

Georgi T. Georgiev, MEMBER SPIE
Science Systems and Applications, Inc.
Lanham, Maryland 20706
E-mail: gtg@spectral.gsfc.nasa.gov

James J. Butler
NASA Goddard Space Flight Center
Code 924
Greenbelt, Maryland 20771

Abstract. Experimental data are presented on the bidirectional reflectance distribution function and 8-deg directional-hemispherical reflectance measurements of a Martian regolith simulant, JSC Mars-1. The scatterometer located in the National Aeronautics and Space Administration's Goddard Space Flight Center Diffuser Calibration Facility was used for the measurements reported. The data were obtained with a monochromator-based light source in the ultraviolet, visible, and near infrared spectral regions. The measurements were performed at different angles of incidence and over a range of in-plane and out-of-plane scattered geometries. The results presented are traceable to the National Institute of Standards and Technology. The hemispherical and diffuse scattering data obtained from these studies are important for current and future Mars space- and ground-based observations. [DOI: 10.1117/1.1870001]

Subject terms: Bidirectional reflectance distribution function; hemispherical reflectance; optical scattering; reflectance spectroscopy; remote sensing.

Paper 040200 received Apr. 8, 2004; revised manuscript received Oct. 8, 2004; accepted for publication Oct. 18, 2004; published online Mar. 10, 2005.

1 Introduction

We present new results on the bidirectional reflectance distribution function (BRDF) and 8-deg directional-hemispherical reflectance of the Martian regolith simulant Johnson Space Center Mars-1 (JSC Mars-1), performed in the Diffuser Calibration Facility (DCaF) at NASA's Goddard Space Flight Center (GSFC). The facility scatterometer,[1] located in a class-10,000 laminar-flow clean room, is a fully automated instrument capable of measuring the BRDF and 8-deg directional-hemispherical reflectance of a wide range of sample types in the spectral range from 230 to 900 nm. The scatterometer can perform in-plane and out-of-plane BRDF measurements with a typical measurement uncertainty of less than 1% (coverage factor $k=1$). The experimental BRDF data were obtained with a monochromator-based Xe short-arc light source over a range of in- and out-of-plane incident and scattered geometries. Data on 8-deg directional-hemispherical reflectance were also measured and are reported here.

The planets are covered with a regolith layer that consists of minerals with differing composition, size, and shape. It is important to know their physical properties and how electromagnetic radiation interacts with these regolith layer components. The physics of incident light transmission, reflection, absorption, and multiple scattering by such regolith layers is complex and is difficult to understand and model. The BRDF characterization of planetary and terrestrial objects is often used in remote sensing applications. To date, a number of semiempirical models for analyzing the BRDF of particulate surfaces have been developed. The Hapke model[2–4] is most widely used in studies of the bidirectional reflectance of regoliths. Liang[5] has proposed a modified Hapke model, and Cord et al.[6] have proposed an optimized determination of Hapke parameters. Mishchenko[7] has indicated that the approximations used in Hapke's model are not appropriate for a close-packed medium. Hillier and Buratti[8] have used a Monte Carlo scattering model for light scattering from a planetary surface.

The JSC-1 Martian regolith simulant sample is the <1-mm-diameter fraction of weathered volcanic ash from Pu'u Nene, a cinder cone on the island of Hawaii, which has been repeatedly cited as a close spectral analog to the bright Mars regions.[9–11] Additional information on the mineralogy,[9] reflectivity spectra,[10] and granulometry[11] has been published.

The results of various experiments involving the Martian regolith simulant on its microbial life,[12] luminescence signals,[13] particle charging,[14] and electrical discharge[15] have been reported in scientific journals. In the current paper we present very precise and accurate BRDF laboratory measurements of the same material. The reported data are intended to more completely describe the optical characteristics of JSC Mars-1 regolith simulant through its diffuse reflectance properties and should be of great interest and value to scientists working on the scattering of planetary regoliths. We have examined our results in reference to well-known scattering models.

2 Background

The BRDF is a fundamental quantity describing the reflectance properties of samples in such different applications as remote sensing,[16] computer graphics,[17] and image interpretation.[18] It describes the variation of reflectance

0091-3286/2005/$22.00

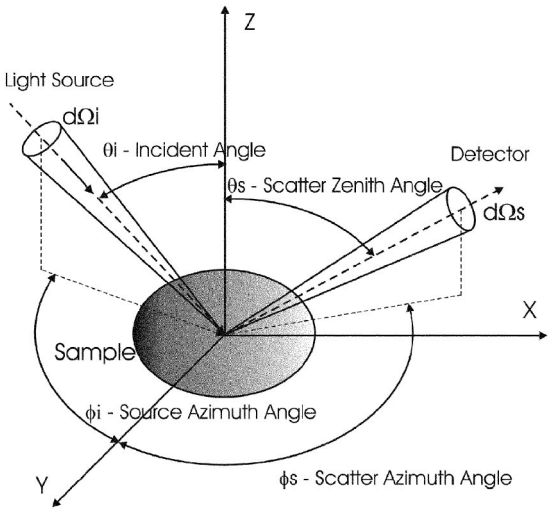

Fig. 1 Defining the BRDF in terms of the usually adopted symbols.

with the illumination and scattered light directions. In many materials the surface reflectance properties are described by both specular and diffuse reflectance.

The BRDF is defined as the ratio of the radiance L_s scattered by a surface into the direction (θ_s, ϕ_s) to the collimated irradiance E_i incident on a unit area of the surface:[19]

$$\mathrm{BRDF} = \frac{L_s(\theta_i, \phi_i, \theta_s, \phi_s, \lambda)}{E_i(\theta_i, \phi_i, \lambda)}, \tag{1}$$

where θ is the zenith angle, ϕ is the azimuth angle, the subscripts i and s are for the incident and scattered directions, respectively, and λ is the wavelength. The BRDF angular convention is presented in Fig. 1.

In practice, the BRDF is usually described in terms of the incident power, the scattered power, and the geometry of the reflected scatter. It is equal to the scattered power per unit solid angle normalized by the product of the incident power and the cosine of the detector view angle:[19]

$$\mathrm{BRDF} = \frac{P_s/\Omega}{P_i \cos\theta_s}, \tag{2}$$

where P_s is the scattered power; Ω is the solid angle determined by the detector aperture area A and the radius R from the sample to the detector $(\Omega = A/R^2)$; P_i is the incident power; and θ_s is the scattering angle.

The scatterometer we used to perform the reported measurements is specified with a combined measurement uncertainty of 1.0% $(k=1)$, which depends on several instrument parameters.[1] The BRDF measurement uncertainty, Δ_{BRDF}, can be evaluated and expressed in accordance with NIST guidelines[20] as

$$(\Delta_{\mathrm{BRDF}})^2 = 2(\Delta_{\mathrm{NS}})^2 + 2(\Delta_{\mathrm{LIN}})^2 + (\Delta_{\mathrm{SLD}})^2 + (\Delta_{\theta s}\tan\theta_s)^2, \tag{3}$$

where Δ_{NS} is the noise-to-signal ratio, Δ_{LIN} represents the nonlinearity of the electronics, Δ_{SLD} is the error of the receiver view angle, $\Delta_{\theta s}$ is the error of the total scattering angle, and θ_s is the error of the receiver scattering angle. The error of the receiver view angle, Δ_{SLD}, is

$$(\Delta_{\mathrm{SLD}})^2 = (2\Delta_{\mathrm{RM}})^2 + (2\Delta_{\mathrm{RZ}})^2 + (2\Delta_{\mathrm{RA}})^2, \tag{4}$$

where Δ_{RM} is the error in the goniometer receiver arm radius, Δ_{RZ} is the error of the receiver arm radius due to sample Z-direction misalignment, and Δ_{RA} is the error of the receiver aperture radius. The total scattering-angle error, $\Delta_{\theta s}$, is given by

$$(\Delta_{\theta s})^2 = (\Delta_{\theta \mathrm{M}})^2 + (\Delta_{\theta Z})^2 + (\Delta_{\theta \mathrm{T}})^2, \tag{5}$$

where $\Delta_{\theta \mathrm{M}}$ is the error of the goniometer scattering angle, $\Delta_{\theta Z}$ is the error due to sample Z-direction misalignment, and $\Delta_{\theta \mathrm{T}}$ is the sample tilt error.

We used an integrating sphere attachment on the scatterometer to measure the 8-deg directional-hemispherical reflectance of JSC Mars-1. The sphere collects and spatially

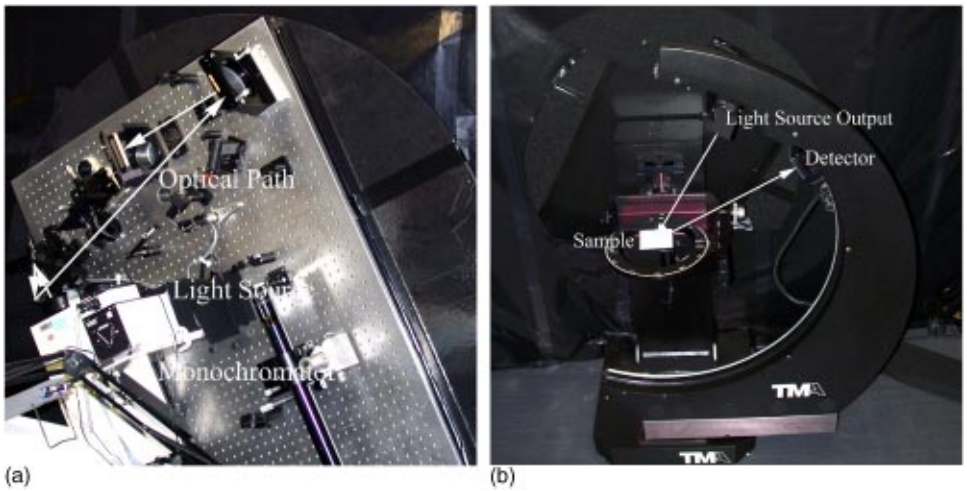

Fig. 2 (a) The scatterometer optical table rotated for 30-deg incident angle. (b) The scatterometer goniometer with the detector at 60-deg zenith and 180-deg azimuth angles.

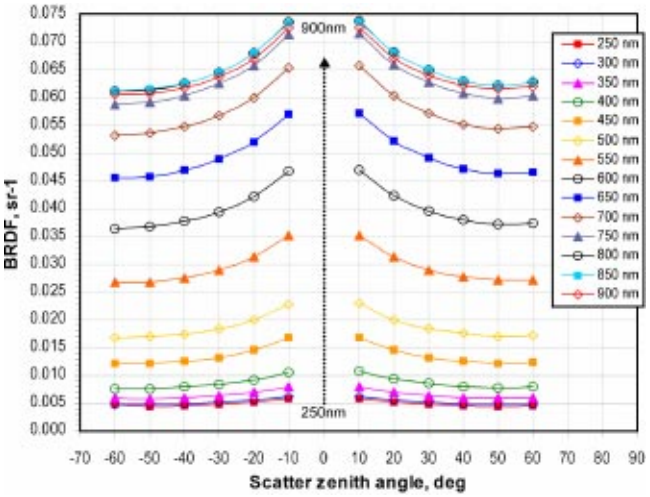

Fig. 3 BRDF at normal incidence, in plane.

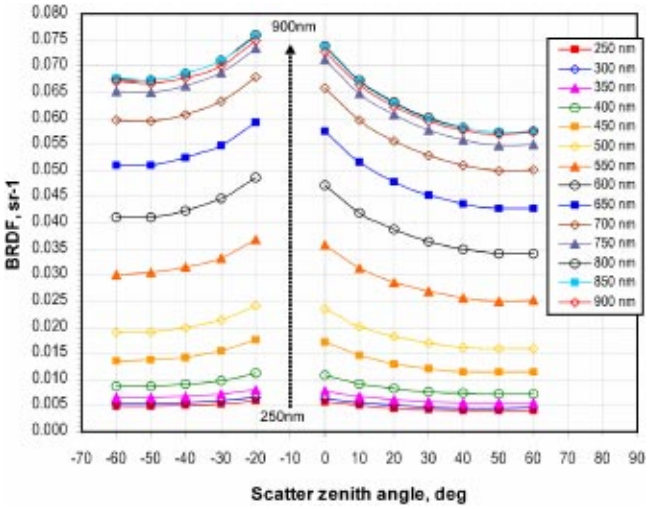

Fig. 5 BRDF at 10-deg incident angle, in plane.

integrates the sample-scattered optical radiation. The sphere interior is made of Spectralon, giving it a high diffuse reflectance over the UV–visible–near-IR region of the spectrum. The reflectance is generally above 99% over a range from 400 to 1500 nm, and above 95% from 250 to 2500 nm. The sphere was designed with four ports, of which three accommodate the sample, the detector, and the entry of the incident light. The fourth port is a spare and is typically closed using a Spectralon plug. The total port area is less than 5% of the total surface area of the sphere, and radiation balance inside the sphere is established after as few internal reflections as possible. The light intensity incident on the detector should correspond to the average light intensity inside the sphere. A silicon photodiode fixed to one port of the sphere was used as a primary detector. The two most important considerations for placing the detector are: (i) the detector should not be directly illuminated by the source, and (ii) the detector should not directly view any part of the sphere wall that is directly illuminated. The detector is supposed to view the part of the sphere wall illuminated by integrated light only. An interior baffle is employed to block the detector from viewing light reflected directly from the sample.

3 Experimental

The scatterometer (Fig. 2), located in a class 10,000 laminar flow clean room, is a fully automated instrument capable of measuring the BRDF of a wide range of sample types in the spectral range from 230 to 900 nm. There are two possible light sources—a 75-W xenon short-arc lamp coupled to a Chromex 250SM scanning monochromator, and a helium-neon laser. Both light source assemblies are mounted on the vertical optical table shown in Fig. 2(a). The table can be rotated around a horizontal axis to change the incident light angle. The monochromatic beam is reflected by a series of spherical and flat mirrors to the sample surface. The beam is mechanically chopped, and a lock-in data acquisition technique is used. The diffuse scattered light is collected using an ultraviolet-enhanced silicon photodiode detector with output fed to a computer-

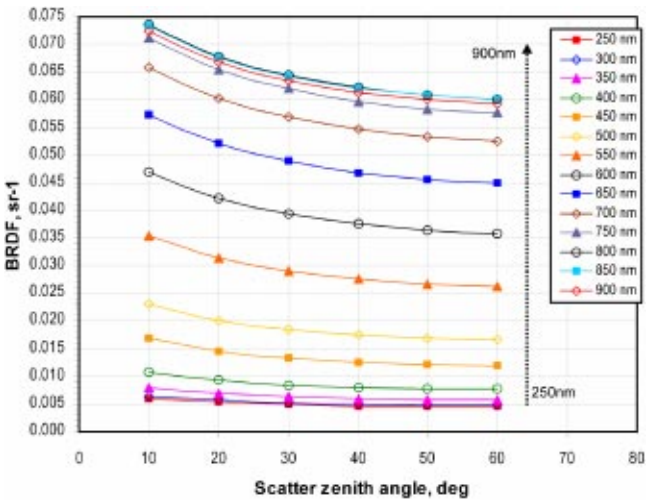

Fig. 4 BRDF at normal incidence, 90 deg out of plane.

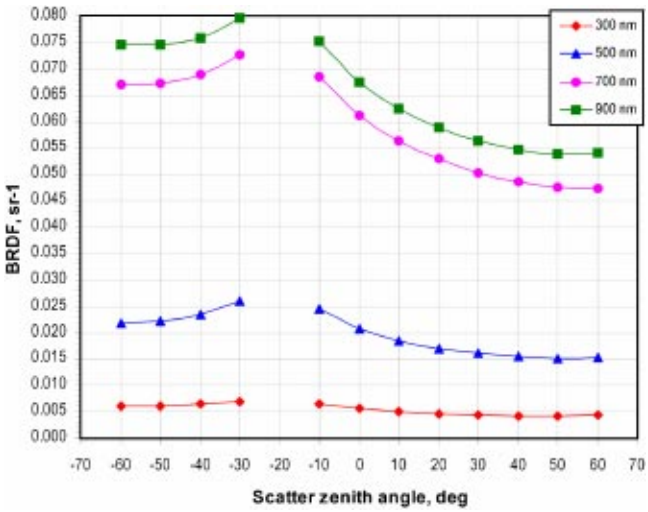

Fig. 6 BRDF at 20-deg incident angle, in plane.

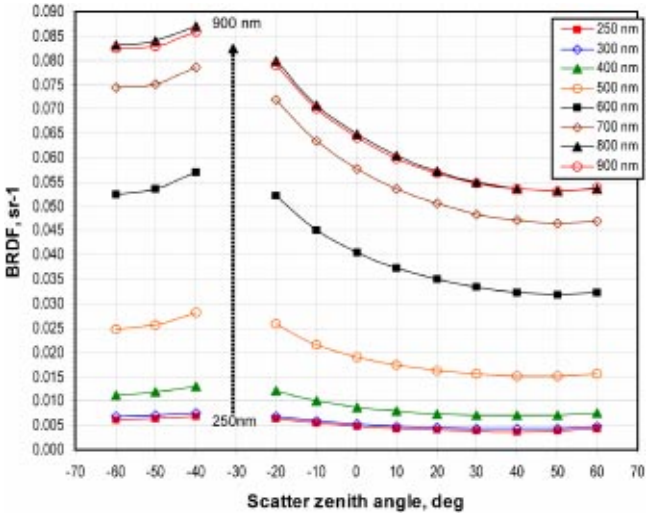

Fig. 7 BRDF at 30-deg incident angle, in plane.

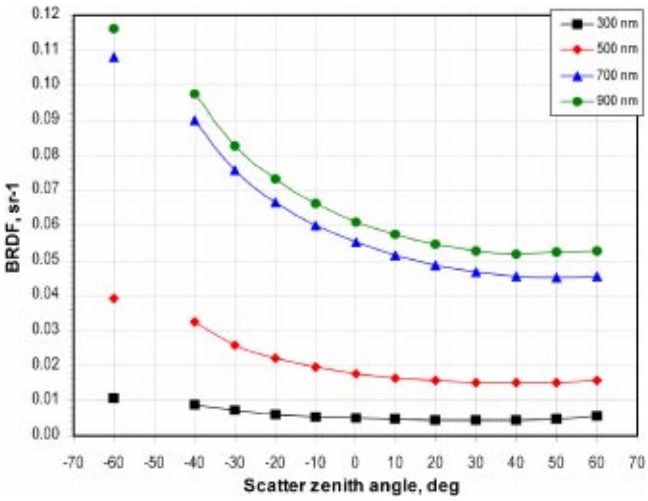

Fig. 9 BRDF at 50-deg incident angle, in plane.

controlled lock-in amplifier. The sample is mounted horizontally as seen in Fig. 2(b), and can be moved in the *X*, *Y*, and *Z* linear directions using three motor stages. There is an additional rotary stage that allows sample rotation in the horizontal plane. The position of the detector assembly is described by the scattering zenith and azimuth angles. The detector assembly can be rotated around the vertical and horizontal axes of the goniometer. Using the sample motor stages, the surface of the sample is positioned at the cross point of the two perpendicular goniometer rotation axes, which define the center of rotation of the goniometer system. The detector field of view, 0.0048 sr, was centered on the calibration item for all measurements and was underfilled by the incident beam, which had a spectral bandwidth of 12 nm. The BRDF is calculated by dividing the net reflected signal by the product of the net incident and the projected solid angle from the sample surface to the detector. Computer-controlled BRDF measurements are acquired at different incident and scattered geometries and wavelengths over the complete scattering hemisphere above the JSC Mars-1 sample. The scatterometer is regularly calibrated using the National Institute of Standards and Technology's (NIST's) Special Tri-function Automated Reference Reflectometer (STARR).[21] The DCaF facility also participates in round-robin test measurements with similar calibration institutions in the USA and abroad in the support of numerous space-flight and non-space-flight programs. The participating institutions, experimental protocol for the EOS BRDF round robin, samples used, and results are published elsewhere.[16] The agreement in BRDF data between the participating institutions depends on the incident and scattered angles, wavelength, and sample.

The experiments were performed at different measurement geometries corresponding to different combinations of incident light angles (0, ±10, 20, ±30, 40, 50, and ±60 deg), scattering azimuth angles (0, 90, and 180 deg), and scattering zenith angles (from 0 to 60 deg in 10-deg steps). The BRDF was measured in the spectral range from 250 up to 900 nm. Measurements were also made with s- and p-linearly-polarized incident beams with the results for unpolarized scattering reported in this paper.

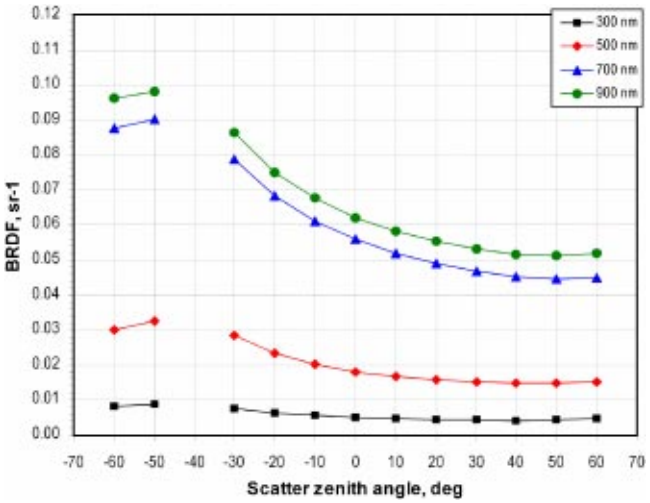

Fig. 8 BRDF at 40-deg incident angle, in plane.

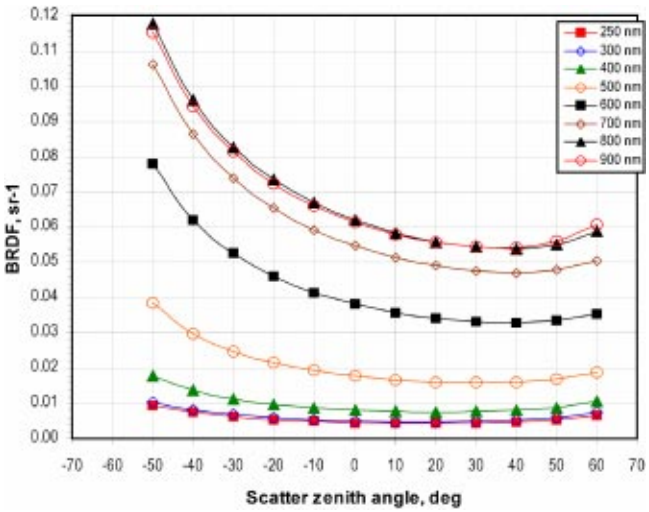

Fig. 10 BRDF at 60-deg incident angle, in plane.

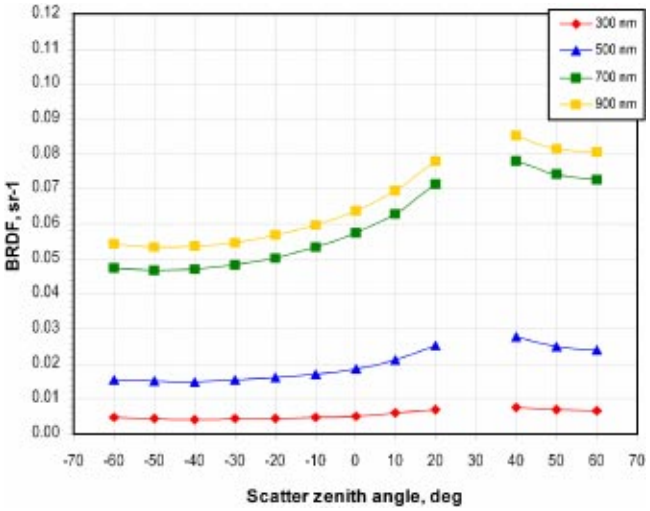

Fig. 11 BRDF at −30-deg incident angle, in plane.

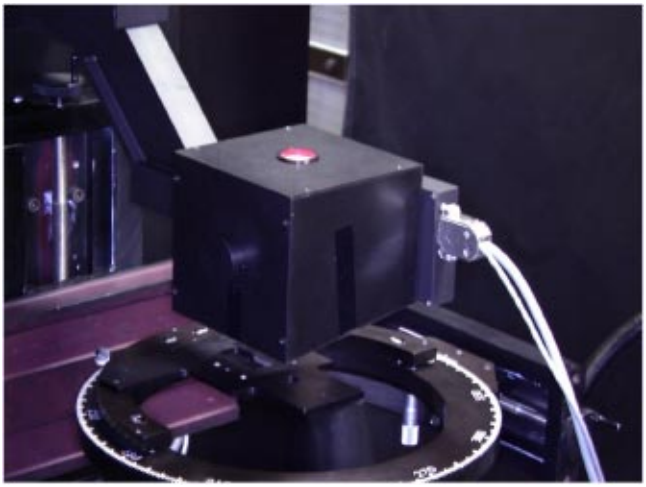

Fig. 12 The 8-deg directional-hemispherical reflectance integrating sphere.

The sample was placed in a black container with dimensions 65×65×5 mm. The container was overfilled, and the sample was flattened without pressure. The size distribution of the particles was the same for the entire surface.

4 Results and Discussion

4.1 *BRDF at Normal Incidence*

The BRDF of JSC Mars-1 was acquired at normal incidence (0-deg incident angle) in the spectral range from 250 to 900 nm every 50 nm. Based on previously measured JSC Mars-1 reflectance spectra,[10] this wavelength interval was determined to be adequate for the study of the spectral dependence of the BRDF. In order to examine the forward, out-of-plane, and backscattering characteristics of JSC Mars-1 under normal incidence, the BRDF was measured at scattering azimuth angles of 0, 90, and 180 deg. The 0-deg angle corresponds to forward scattering, 180 deg to backward scattering, and 90 deg to out-of-plane scattering. The scattering zenith angles ranged from 0 to 60 deg in 10-deg steps. The measured curves are shown in Fig. 3 for the 0- and 180-deg scattering azimuth angles, and in Fig. 4 for the 90-deg scattering azimuth angle. Numerical data used in Figs. 3 and 4 are provided in Table 4 of the appendix to this paper. BRDF values of zero indicate that the scatterometer detector's view of the sample was being obscured by the last light-source mirror. It is evident from Figs. 3 and 4 that the BRDF at 900 nm is lower than those at 800 and 850 nm. This can be attributed to the well-known ferric absorption band of the material in the 800–900-nm spectral range. Consistent with previously reported spectral reflectance, the BRDF of JSC Mars-1 increases slowly from 250 to 400 nm and more rapidly above 400 nm until reaching the ferric absorption feature. The BRDF of JSC Mars-1 is independent of scattering azimuth angle at normal incidence (Table 4). It depends on the scattering zenith angle (Fig. 3), decreasing with increasing zenith angle from 0 to 60 deg. The very small differences in BRDF values are of a magnitude less than the scatterometer measurement uncertainty of 1% and are most likely due to subtle nonlevel features in the granular JSC Mars-1 sample.

4.2 *BRDF at Nonnormal Angles of Incidence*

The BRDF of the Mars regolith sample was also measured at nonnormal incident angles of incidence equal to ±10, 20, ±30, 40, 50, and ±60 deg at a number of wavelengths. According to Fig. 1, the incident angle is positive when the light source is rotated clockwise from normal incidence (0 deg) to the corresponding angle, and negative when it is

Table 1 JSC Mars-1 backscattering ratio.

Scattering zenith angle (deg)		Backscattering ratio											
Back (180-deg azimuth)	Forward (0-deg azimuth)	Incident angle 10				30				50 deg			
		Wavelength 300	500	700	900	300	500	700	900	300	500	700	900 nm
−60	60	1.156	1.195	1.190	1.167	1.438	1.588	1.590	1.528	1.904	2.455	2.369	2.198
−50	50	1.185	1.204	1.189	1.168	1.637	1.707	1.620	1.561				
−40	40	1.226	1.232	1.192	1.175	1.779	1.862	1.668	1.607	1.923	2.151	1.979	1.883
−30	30	1.275	1.260	1.196	1.179					1.585	1.703	1.620	1.568
−20	20	1.317	1.324	1.221	1.202	1.560	1.593	1.426	1.392	1.359	1.403	1.367	1.340
−10	10					1.234	1.243	1.184	1.171	1.155	1.178	1.166	1.155

Table 2 Polynomial coefficients.

Wavelength (nm)	*A*	*B*	*C*	*D*
300	-9.82894×10^{-4}	0.29122	−0.02605	1.66337×10^{-3}
400	3.3807×10^{-3}	1.19283	−0.45809	0.10327
500	4.0201×10^{-3}	0.34171	−0.03957	2.58476×10^{-3}
600	4.90461×10^{-3}	0.38612	−0.05035	3.61316×10^{-3}
700	5.70006×10^{-3}	0.56125	−0.10729	0.01139
800	6.15911×10^{-3}	1.03389	−0.36472	0.07069
900	4.33566×10^{-3}	0.1615	-8.66674×10^{-3}	2.43788×10^{-4}

rotated counterclockwise. The values of the incident angles at which measurements were made were chosen to be broad enough for best characterization of BRDF properties of the material. The change in BRDF of diffuse reflective materials due to the incident angle is smooth, and a step of 10 deg is usually used for materials characterization. The BRDF data at positive incident angles are shown in Figs. 5 through 10. The BRDF is plotted at only one negative incident angle, −30 deg, (Fig. 11), because the data mirror those at positive incident angles and corresponding scattering geometries. In Figs. 5 through 11, the detected signal is zero when the detector scattering zenith angle is equal to the incident angle, that is, when the output mirror of the optical system obscured the detector's field of view of the sample. In Fig. 5, the BRDF at 10-deg incidence was recorded every 50 nm from 250 to 900 nm. The BRDF at 20, 40, and 50-deg incidence, shown in Figs. 6, 8, and 9, respectively, was measured from 300 to 900 nm in 200-nm steps. The BRDF at 30- and 60-deg incidence, shown in Figs. 7 and 10, was measured at 250 and 300 nm and thence every 100 nm up to 900 nm. All data were recorded at scattering zenith angles from 0 to 60 deg in 10-deg steps. The numerical data in these figures are given in the appendix (Tables 4 through 10).

The experimental data on the Mars JSC-1 regolith simulant acquired at nonnormal angles of incidence support the claim of appreciable backscattering by the JSC Mars-1 planetary regolith.[22] The backscattering is obtained by simply taking the difference of the BRDF at scattering angles symmetric to the sample normal. These scattering data are compared with the forward-scattering data, and the ratio is given in Table 1 at three wavelengths, 500, 700, and 900 nm, for incident angles of 10, 30, and 50 deg. In this table a positive scattering azimuth angle refers to forward scattering and a negative one to backward scattering. In Tables 5 through 10 the 0-deg scattering azimuth refers to forward scattering, and the 180-deg azimuth to backward scattering. The backscattering is generally higher at higher scattering zenith angles and larger incident light angles. There is also wavelength dependence; the largest difference is registered at 500 nm for corresponding measurement geometry. It reaches a maximum of 2.455 at 500 nm, with 50-deg incident and 60-deg scattering zenith angle. The lowest value, 1.155, was measured at 300 and 900 nm at 50-deg incident and 10-deg scattering zenith angles. The values in Table 1 are computer-generated from the measured data and rounded. The BRDF data presented in the tables for all measurement geometries are rounded to the third decimal for better handling. As a consequence, the backward-forward difference presented in Table 1 cannot be derived independently from the BRDF data tables.

Table 3 JSC Mars-1 8-deg directional-hemispherical reflectance.

Wavelength (nm)	Hemispherical reflectance
300	0.04269
400	0.04655
500	0.05093
600	0.10187
700	0.14445
800	0.1623
900	0.15908

The BRDF increases from shorter to longer wavelengths at nonnormal incident angles. The ferric absorption band in the 800–900-nm spectral region is also present.

The BRDF at nonnormal incident angles depends on the scattering zenith angles in addition to the backscattering already mentioned. It decreases with increasing scattering zenith angles at the same incident angle and wavelength. The BRDF depends also on the scattering azimuth angle. It is lower on the forward branch of in-plane scattering (0-deg scattering azimuth), higher for 90-deg out-of-plane scattering (90-deg scattering azimuth), and highest on the backward branch of in-plane (180-deg scattering azimuth) scattering geometry (Table 5).

The validity and application of Helmholtz reciprocity[23] to BRDF are well known and modeled for both flat and structured surfaces. According to that principle, we can exchange the incident and scattering angles without change in the BRDF. In our in-plane setup the BRDFs measured at positive incident angles and 0-deg scattering azimuth mirror those measured at negative incident angles and 180-deg scattering azimuth for the same wavelengths and scattering zenith angles with respect to our angle sign convention. Two of our reciprocal measurement points—evidence for reliable experimental BRDF data—are compared as follows: the BRDF at 500 nm, 40-deg, incident angle, and −30-deg scattering zenith angle (Fig. 8) is 0.028 sr^{-1}, and the BRDF at the same wavelength, −30-deg incident angle, and 40-deg scattering zenith angle is again 0.028 sr^{-1} (Fig. 11).

Table 4 JSC Mars-1 BRDF at normal incidence.

Scattering zenith angle (deg)	BRDF											
	Scattering azimuth angle 0	90	180	0	90	180	0	90	180	0	90	180 deg
	250 nm			300 nm			350 nm			400 nm		
0	0.000	0.000	0.000	0.000	0.000	0.000	0.000	0.000	0.000	0.000	0.000	0.000
10	0.006	0.006	0.006	0.006	0.006	0.006	0.008	0.008	0.008	0.011	0.011	0.011
20	0.005	0.005	0.005	0.006	0.006	0.006	0.007	0.007	0.007	0.009	0.009	0.009
30	0.005	0.005	0.005	0.005	0.005	0.005	0.006	0.006	0.006	0.009	0.008	0.008
40	0.005	0.005	0.005	0.005	0.005	0.005	0.006	0.006	0.006	0.008	0.008	0.008
50	0.004	0.005	0.004	0.005	0.005	0.005	0.006	0.006	0.006	0.008	0.008	0.008
60	0.005	0.005	0.005	0.005	0.005	0.005	0.006	0.006	0.006	0.008	0.008	0.008
	450 nm			500 nm			550 nm			600 nm		
0	0.000	0.000	0.000	0.000	0.000	0.000	0.000	0.000	0.000	0.000	0.000	0.000
10	0.017	0.017	0.017	0.023	0.023	0.023	0.035	0.035	0.035	0.047	0.047	0.047
20	0.015	0.015	0.015	0.020	0.020	0.020	0.031	0.031	0.031	0.042	0.042	0.042
30	0.013	0.013	0.013	0.018	0.018	0.018	0.029	0.029	0.029	0.040	0.039	0.039
40	0.013	0.012	0.013	0.018	0.017	0.017	0.028	0.028	0.028	0.038	0.038	0.038
50	0.012	0.012	0.012	0.017	0.017	0.017	0.027	0.027	0.027	0.037	0.036	0.037
60	0.012	0.012	0.012	0.017	0.017	0.017	0.027	0.026	0.027	0.037	0.036	0.036
	650 nm			700 nm			750 nm			800 nm		
0	0.000	0.000	0.000	0.000	0.000	0.000	0.000	0.000	0.000	0.000	0.000	0.000
10	0.057	0.057	0.057	0.066	0.066	0.065	0.072	0.071	0.071	0.074	0.074	0.074
20	0.052	0.052	0.052	0.060	0.060	0.060	0.066	0.065	0.066	0.068	0.068	0.068
30	0.049	0.049	0.049	0.057	0.057	0.057	0.063	0.062	0.063	0.065	0.065	0.065
40	0.047	0.047	0.047	0.055	0.055	0.055	0.061	0.060	0.060	0.063	0.062	0.063
50	0.046	0.046	0.046	0.054	0.053	0.054	0.060	0.058	0.059	0.062	0.061	0.061
60	0.047	0.045	0.046	0.055	0.053	0.053	0.060	0.058	0.059	0.063	0.060	0.061
	850 nm			900 nm								
0	0.000	0.000	0.000	0.000	0.000	0.000						
10	0.074	0.073	0.073	0.073	0.072	0.073						
20	0.068	0.068	0.068	0.067	0.067	0.067						
30	0.065	0.064	0.065	0.064	0.063	0.064						
40	0.063	0.062	0.063	0.062	0.061	0.062						
50	0.062	0.061	0.062	0.062	0.060	0.061						
60	0.063	0.060	0.061	0.062	0.059	0.061						

4.3 *The 8-deg Directional-Hemispherical Setup and Measurements*

The 8-deg directional-hemispherical reflectance of JSC Mars-1 was measured at wavelengths of 300, 400, 500, 600, 700, 800, and 900 nm using the same monochromatic light source as with the BRDF measurements. The only hardware difference from the experimental setup described in the previous section is the use of an 8-deg directional-hemispherical integrating sphere assembly mounted above the scatterometer sample stage, as shown in Fig. 12. The silicon photodiode detector was fixed to the port of the sphere on the right. The dependence of the hemispherical reflectance versus receiver power is fitted using a third-degree polynomial regression:

$$R(P)=A+BP-CP^2+DP^3. \tag{6}$$

The coefficients of the polynomial can be calculated by fitting the receiver power measured using a set of seven gray Spectralon standard plates with known 8-deg directional-hemispherical reflectance. With the setup described, the power was measured at each wavelength of interest for each standard plate, and the coefficients were calculated using a third-degree polynomial fitting procedure. The coefficients calculated are given in Table 2, and the measured 8-deg directional-hemispherical data on JSC Mars-1 are given in Table 3. To verify the proposed procedure we compared the Labsphere-measured and our measured 8-deg directional-hemispherical reflectance values of

Table 5 JSC Mars-1 BRDF at 10-deg incidence.

Scattering zenith angle (deg)	BRDF											
	Scattering azimuth angle 0	90	180	0	90	180	0	90	180	0	90	180 deg
	250 nm			300 nm			350 nm			400 nm		
0	0.006	0.006	0.006	0.006	0.006	0.006	0.008	0.008	0.008	0.011	0.011	0.011
10	0.005	0.005	0.000	0.006	0.006	0.000	0.007	0.007	0.000	0.009	0.010	0.000
20	0.004	0.005	0.006	0.005	0.005	0.007	0.006	0.007	0.008	0.008	0.009	0.011
30	0.004	0.004	0.005	0.005	0.005	0.006	0.006	0.006	0.007	0.008	0.008	0.010
40	0.004	0.004	0.005	0.004	0.005	0.006	0.005	0.006	0.007	0.007	0.008	0.009
50	0.004	0.004	0.005	0.004	0.005	0.005	0.005	0.006	0.007	0.007	0.008	0.009
60	0.004	0.004	0.005	0.005	0.005	0.005	0.005	0.006	0.006	0.007	0.008	0.009
	450 nm			500 nm			550 nm			600 nm		
0	0.017	0.017	0.017	0.023	0.023	0.023	0.036	0.036	0.036	0.047	0.047	0.047
10	0.015	0.016	0.000	0.020	0.022	0.000	0.031	0.034	0.000	0.042	0.045	0.000
20	0.013	0.014	0.018	0.018	0.020	0.024	0.029	0.031	0.037	0.039	0.042	0.049
30	0.012	0.013	0.015	0.017	0.019	0.021	0.027	0.029	0.033	0.036	0.039	0.045
40	0.012	0.013	0.014	0.016	0.018	0.020	0.026	0.028	0.031	0.035	0.038	0.042
50	0.011	0.012	0.014	0.016	0.017	0.019	0.025	0.027	0.030	0.034	0.037	0.041
60	0.011	0.012	0.014	0.016	0.017	0.019	0.025	0.027	0.030	0.034	0.036	0.041
	650 nm			700 nm			750 nm			800 nm		
0	0.058	0.058	0.058	0.066	0.066	0.066	0.071	0.071	0.071	0.074	0.074	0.074
10	0.052	0.055	0.000	0.060	0.063	0.000	0.065	0.069	0.000	0.067	0.071	0.000
20	0.048	0.051	0.059	0.056	0.059	0.068	0.061	0.065	0.073	0.063	0.067	0.076
30	0.045	0.049	0.055	0.053	0.056	0.063	0.058	0.062	0.069	0.060	0.064	0.071
40	0.044	0.047	0.052	0.051	0.054	0.061	0.056	0.060	0.066	0.058	0.062	0.069
50	0.043	0.046	0.051	0.050	0.053	0.059	0.055	0.058	0.065	0.057	0.060	0.067
60	0.043	0.045	0.051	0.050	0.052	0.060	0.055	0.058	0.065	0.058	0.060	0.068
	850 nm			900 nm								
0	0.074	0.074	0.074	0.073	0.073	0.073						
10	0.067	0.070	0.000	0.066	0.070	0.000						
20	0.063	0.067	0.076	0.062	0.066	0.075						
30	0.060	0.064	0.071	0.059	0.063	0.070						
40	0.058	0.062	0.069	0.058	0.061	0.068						
50	0.057	0.060	0.067	0.057	0.060	0.067						
60	0.058	0.060	0.068	0.057	0.059	0.067						

Spectralon samples of nominal reflectance 5%, 10%, 20%, 40%, 60%, 80%, and 99%. It was found that the difference between the two measurements is better than $\pm 1\%$ for the entire spectral range of interest.

5 Conclusions

The BRDF and 8-deg directional-hemispherical reflectance of the Martian regolith simulant JSC Mars-1 were measured in the UV, visible, and near-IR spectral regions. The sample exhibits a wide range of BRDF values depending on the scattering geometry. Different angles of incidence from 0 to 60 deg, scattering zenith angles from 0 to 60 deg, and scattering azimuth angles 0, 90, and 180 deg were used for the full characterization of the sample. The reported experimental data show a flat BRDF response in the UV with increasing deviation from the Lambertian at higher wavelengths. The BRDF depends on both the incident and scattered light angles. The difference can be up to 13.88% for a 10-deg change of the scattering zenith angle at 500 nm. The BRDF at all wavelengths measured is symmetrical to the normal at normal incidence. Strong optical backscattering from the sample is detected, supporting the planetary regolith simulant scattering models as presented by some authors.[22] The reciprocity of the BRDF is confirmed for the material. Some 8-deg directional-hemispherical measurements are also presented. They give additional data on the material reflectance properties. The diffuse-scattering and 8-deg directional-hemispherical data from

Table 6 JSC Mars-1 BRDF at 20-deg incidence.

Scattering zenith angle (deg)	BRDF							
	Scattering azimuth angle 0	180	0	180	0	180	0	180 deg
	300 nm		500 nm		700 nm		900 nm	
0	0.006	0.006	0.021	0.021	0.061	0.061	0.067	0.067
10	0.005	0.007	0.019	0.024	0.056	0.069	0.062	0.075
20	0.005	0.000	0.017	0.000	0.053	0.000	0.059	0.000
30	0.004	0.007	0.016	0.026	0.050	0.073	0.056	0.080
40	0.004	0.006	0.015	0.023	0.049	0.069	0.055	0.076
50	0.004	0.006	0.015	0.022	0.047	0.067	0.054	0.075
60	0.004	0.006	0.015	0.022	0.047	0.067	0.054	0.075

Table 7 JSC Mars-1 BRDF at 30-deg incidence.

Scattering zenith angle (deg)	BRDF							
	Scattering azimuth angle 0	180	0	180	0	180	0	180 deg
	300 nm		400 nm		500 nm		600 nm	
0	0.005	0.005	0.009	0.009	0.019	0.019	0.041	0.041
10	0.005	0.006	0.008	0.010	0.017	0.022	0.037	0.045
20	0.004	0.007	0.007	0.012	0.016	0.026	0.035	0.052
30	0.004	0.000	0.007	0.000	0.015	0.000	0.033	0.000
40	0.004	0.008	0.007	0.013	0.015	0.028	0.032	0.057
50	0.004	0.007	0.007	0.012	0.015	0.026	0.032	0.054
60	0.005	0.007	0.007	0.011	0.016	0.025	0.032	0.052
	700 nm		800 nm		900 nm			
0	0.058	0.058	0.065	0.065	0.064	0.064		
10	0.054	0.063	0.060	0.071	0.060	0.070		
20	0.050	0.072	0.057	0.080	0.057	0.079		
30	0.048	0.000	0.055	0.000	0.055	0.000		
40	0.047	0.079	0.054	0.087	0.053	0.086		
50	0.046	0.075	0.053	0.084	0.053	0.083		
60	0.047	0.075	0.054	0.083	0.054	0.082		

Table 8 JSC Mars-1 BRDF at 40-deg incidence.

Scattering zenith angle (deg)	BRDF							
	Scattering azimuth angle 0	180	0	180	0	180	0	180 deg
	300 nm		500 nm		700 nm		900 nm	
0	0.005	0.005	0.018	0.018	0.056	0.056	0.062	0.062
10	0.005	0.006	0.017	0.020	0.052	0.061	0.058	0.068
20	0.004	0.006	0.016	0.023	0.049	0.068	0.055	0.075
30	0.004	0.008	0.015	0.028	0.047	0.079	0.053	0.086
40	0.004	0.000	0.015	0.000	0.045	0.000	0.052	0.000
50	0.004	0.009	0.015	0.032	0.045	0.090	0.051	0.098
60	0.005	0.008	0.015	0.030	0.045	0.088	0.052	0.096

Table 9 JSC Mars-1 BRDF at 50-deg incidence.

Scattering zenith angle (deg)	BRDF							
	Scattering azimuth angle 0	180	0	180	0	180	0	180 deg
	300 nm		500 nm		700 nm		900 nm	
0	0.005	0.005	0.018	0.018	0.055	0.055	0.061	0.061
10	0.005	0.005	0.017	0.019	0.052	0.060	0.057	0.066
20	0.004	0.006	0.016	0.022	0.049	0.067	0.055	0.073
30	0.004	0.007	0.015	0.026	0.047	0.076	0.053	0.083
40	0.005	0.009	0.015	0.032	0.045	0.090	0.052	0.098
50	0.005	0.000	0.015	0.000	0.045	0.000	0.052	0.000
60	0.006	0.011	0.016	0.039	0.046	0.108	0.053	0.116

Table 10 JSC Mars-1 BRDF at 60-deg incidence.

Scattering zenith angle (deg)	BRDF							
	Scattering azimuth angle 0	180	0	180	0	180	0	180 deg
	300 nm		400 nm		500 nm		600 nm	
0	0.005	0.005	0.008	0.008	0.018	0.018	0.038	0.038
10	0.005	0.005	0.008	0.009	0.017	0.019	0.036	0.041
20	0.005	0.006	0.008	0.010	0.016	0.021	0.034	0.046
30	0.005	0.007	0.008	0.011	0.016	0.025	0.033	0.053
40	0.005	0.008	0.008	0.014	0.016	0.030	0.033	0.062
50	0.006	0.010	0.009	0.018	0.017	0.039	0.033	0.078
60	0.007	0.000	0.011	0.000	0.019	0.000	0.035	0.000
	700 nm		800 nm		900 nm			
0	0.055	0.055	0.062	0.062	0.061	0.061		
10	0.051	0.059	0.058	0.067	0.058	0.066		
20	0.049	0.066	0.056	0.074	0.056	0.072		
30	0.048	0.074	0.054	0.083	0.054	0.081		
40	0.047	0.086	0.054	0.096	0.054	0.094		
50	0.048	0.106	0.055	0.118	0.056	0.115		
60	0.050	0.000	0.059	0.000	0.061	0.000		

these studies are important for the analysis of spectral data obtained at future Mars space- and ground-based observations. They can be also used for calibration of existing data. The high quality of the data is supported by the fact that the measurements were done on a high-accuracy scatterometer located in a clean-room calibration facility and the results are traceable to the measurements made at NIST.

6 Appendix

The BRDF data on the Mars JSC-1 regolith simulant are presented numerically in Tables 4–10.

References

1. T. F. Schiff, M. W. Knighton, D. J. Wilson, F. M. Cady, J. C. Stover, and J. J. Butler, ''A design review of a high accuracy UV to near infrared scatterometer,'' *Proc. SPIE* **1995**, 121–130 (1993).
2. B. Hapke, ''Bidirectional reflectance spectroscopy 1. Theory,'' *J. Geophys. Res.* **86**, 3039–3054 (1981).
3. B. Hapke, *Theory of Reflectance and Emittance Spectroscopy*, Cambridge Univ. Press, Cambridge, UK (1993).
4. B. Hapke, ''Bidirectional reflectance spectroscopy 5. The coherent backscatter opposition effect and anisotropic scattering,'' *Icarus* **157**, 523–534 (2002).
5. S. Liang and J. R. G. Townshend, ''A modified Hapke model for soil bidirectional reflectance,'' *Remote Sens. Environ.* **55**, 1–10 (1996).
6. A. M. Cord, P. C. Pinet, Y. Daydou, and S. D. Chevrel, ''Planetary regolith surface analogs: optimized determination of Hapke parameters using multi-angular spectro-imaging laboratory data,'' *Icarus* **165**, 414–427 (2003).
7. M. I. Mishchenko, ''Asymmetry parameters of the phase function for densely packed scattering grains,'' *J. Quant. Spectrosc. Radiat. Transf.* **52**, 95–110 (1994).
8. J. K. Hillier and B. J. Buratti, ''Monte Carlo simulations of light scattering by composite particles in a planetary surface,'' *Icarus* **149**, 251–261 (2001).
9. R. V. Morris, D. C. Golden, J. F. Bell, H. V. Lauer, and J. B. Adams, ''Pigmenting agents in Martian soils: inferences from spectral, Mössbauer and magnetic properties of nanophase and other iron oxides in

Hawaiian palagonitic soil PN-9*,'' *Geochim. Cosmochim. Acta* **57**, 4597–4609 (1993).
10. C. C. Allen, R. V. Morris, D. J. Lindstrom, M. M. Lindstrom, and J. P. Lockwood, ''JSC Mars-1: Martian regolith simulant,'' presented at Lunar and Planetary Science XXVIII, 1997, Paper 1797, Lunar and Planetary Institute.
11. C. C. Allen, R. V. Morris, K. M. Jager, D. C. Golden, D. J. Lindstrom, M. M. Lindstrom, and J. P. Lockwood, ''Martian regolith simulant JSC Mars-1,'' presented at Lunar and Planetary Science XXIX, 1998, Paper 1954, Lunar and Planetary Institute.
12. C. C. Allen, C. Griffin, A. Steele, N. Wainwright, and E. Stansbery, ''Microbial life in Martian regolith simulant JSC Mars-1,'' presented at Lunar and Planetary Science XXXI, 2000, Paper 1287, Lunar and Planetary Institute.
13. D. Banerjee, M. Blair, K. Lepper, and S. W. S. McKeever, ''Optically stimulated luminescence signals of polymineral fine grains in the JSC Mars-1 soil simulant sample,'' *Radiat. Protection Dosimetry* **101**, 321–326 (2002).
14. F. B. Gross, ''JSC Mars-1 Martian regolith simulant particle charging experiments in the presence of AC and DC corona fields,'' *J. Electrost.* **58**, 147–156 (2003).
15. A. Fabian, C. Krauss, A. Sickafoose, M. Horanyi, and S. Robertson, ''Measurements of electrical discharges in Martian regolith simulant,'' *IEEE Trans. Plasma Sci.* **29**, 288–291 (2001).
16. E. A. Early, P. Y. Barnes, B. C. Johnson, J. J. Butler, C. J. Bruegge, S. F. Biggar, P. S. Spyak, and M. M. Pavlov, ''Bidirectional reflectance round-robin in support of the Earth Observing System Program,'' *J. Atmos. Ocean. Technol.* **17**, 1077–1091 (2000).
17. N. Noe and B. Peroche, ''Hierarchical reconstruction of BRDFs using locally supported functions,'' *Computer Graph. Forum* **19**, 173–184 (2000).
18. S. R. Marschner, S. H. Westin, E. P. F. Lafortune, and K. E. Torrance, ''Image-based bidirectional reflectance distribution function measurement,'' *Appl. Opt.* **39**, 2592–2600 (2000).
19. F. E. Nicodemus, J. C. Richmond, J. J. Hsia, I. W. Ginsburg, and T. Limperis, ''Geometrical considerations and nomenclature for reflectance,'' NBS monograph 160, National Bureau of Standards (1977).
20. B. N. Taylor and C. E. Kuyatt, ''A guideline for evaluating and expressing the uncertainty of NIST measurement results,'' NIST Technical Note 1297, U.S. Department of Commerce, National Institute of Standards and Technology (1997).
21. J. R. Proctor and P. Y. Barnes, ''NIST high accuracy reference reflectometer–spectrophotometer,'' *J. Res. Natl. Inst. Stand. Technol.* **101**, 619–627 (1996).
22. B. Hapke, ''Scattering and diffraction of light by particles in planetary regoliths,'' *J. Quant. Spectrosc. Radiat. Transf.* **61**, 565–581 (1999).
23. F. J. J. Clarke and D. J. Parry, ''Helmholtz reciprocity: its validity and application to reflectometry,'' *Light. Res. Technol.* **17**, 1–11 (1985).

Georgi T. Georgiev studied at the Budapest Technical University, where he graduated with a diploma in engineering in 1982. He received his PhD in physics from the Bulgarian Academy of Sciences in 1998. He was associated for two years with the University of Maryland, where he worked on NASA's Goddard Space Flight Center projects on acousto-optic imaging spectroscopy for space applications. He is currently with Science Systems and Applications, Inc., and the Calibration Facility of NASA's Goddard Space Flight Center, Greenbelt, Maryland. His main current research interests are in the fields of optical scattering and diffraction. He is involved in instrument development and measurements of bidirectional scattering distribution functions (BSDFs) in the ultraviolet through near-infrared wavelength regions on a variety of optical and nonoptical materials. His publications reflect research interests in optical scattering and acousto-optic devices. He is a member of SPIE and OSA.

James J. Butler received his BS degree in physical chemistry from the University of Notre Dame, Notre Dame, IN, in 1977, and the PhD degree in physical chemistry from the University of North Carolina at Chapel Hill in 1982. He is currently an optical physicist in the Laboratory for Terrestrial Physics's Laser Remote Sensing Branch at NASA's Goddard Space Flight Center (GSFC), where he has been a research scientist since 1984. Since January 1995 and January 2003, he has performed the duties of EOS calibration scientist and of NASA's representative to the NPOESS Joint Agency Requirements Group (JARG), respectively. Since June 2004, he has performed the duties of NASA's deputy project scientist for instruments and calibration within the NPOESS Preparatory Project (NPP). He also manages the NASA/GSFC diffuser calibration facility. His previous research experience at NASA includes ground-based and balloon-borne lidar for the detection of stratospheric molecular and radical species and laser-induced fluorescence of molecules and radicals.